REPORT

UEA MTH / IFR Study Group Workshop

14–16 September 2009

Contents

2 Proposed Problems

The following proposed problems fall into one of two classes:

A) a clearly defined question where a reasonably well-formed mathematical statement already exists that is supported by a more-or-less extensive published literature;

B) an incomplete list of scientific facts and some vaguely formulated hypotheses suggesting how these results might be organised into a quantitative theory, with little or no identifiable literature.

It is anticipated that problems of class (A) might succumb to significant analytic progress during the Workshop while problems of class (B) are likely to benefit most from the development of simple feature definitions and model statements. Within each class, the following lists are presented in order of *decreasing* priority from the IFR perspective. This should not wholly determine the choice of problems to focus on, but should be a consideration nevertheless.

2.1 Class (A)

2.1.1 Dynamic interface rheology studied by atomic force microscopy (AFM) (R. Penfold)

Carnie et al. (*Langmuir*, **21**(7), 2912–2922, 2005) have formulated and verified a complete mathematical theory predicting the force between a single pair of axisymmetric emulsion droplets measured by AFM as a function of interface separation $h(r,t)$. The theory accounts for:

- surface forces (Coulomb interactions primarily);
- hydrodynamic drainage of the intervening thin film;
- axisymmetric droplet deformation (small);
- AFM cantilever deflection.

A novel boundary condition for the thinning equation (Reynolds) arises by matching asymptotic expansions for the droplet profiles $z(r,t)$ between the "interaction zone" of radial scale hR_0 and the far-field. On discretisation, this leads to a differential-algebraic equation system (of index 1), rather than a pure ODE system, but endows the calculation with the key feature of numerical stability with respect to choice of radial cut-off distance. This theory has been implemented at IFR (Matlab) and performs in agreement with the reported results.

An important assumption of model characterises the interfaces by only their static tension coefficient. Furthermore, it is supposed that considerable amounts of surfactant have been adsorbed to each interface, forming an *immobile* layer that resists the transmission of tangential stress between the continuous phase flow and the droplet fluid. A no-slip boundary condition is applied. For small molecule ionic surfactants at high concentration, these assumptions and the corresponding theory yield predictions in very good agreement with experimental measurements. This has also been confirmed by work at IFR.

With protein emulsifiers or large non-ionic surfactants, however, forces measured by the IFR team are at some variance with the model predictions. The assumptions of negligible interfacial rheology and immobile interfacial structure are believed to be the cause of this discrepancy. There is a need to modify the Carnie et al. analysis accordingly.

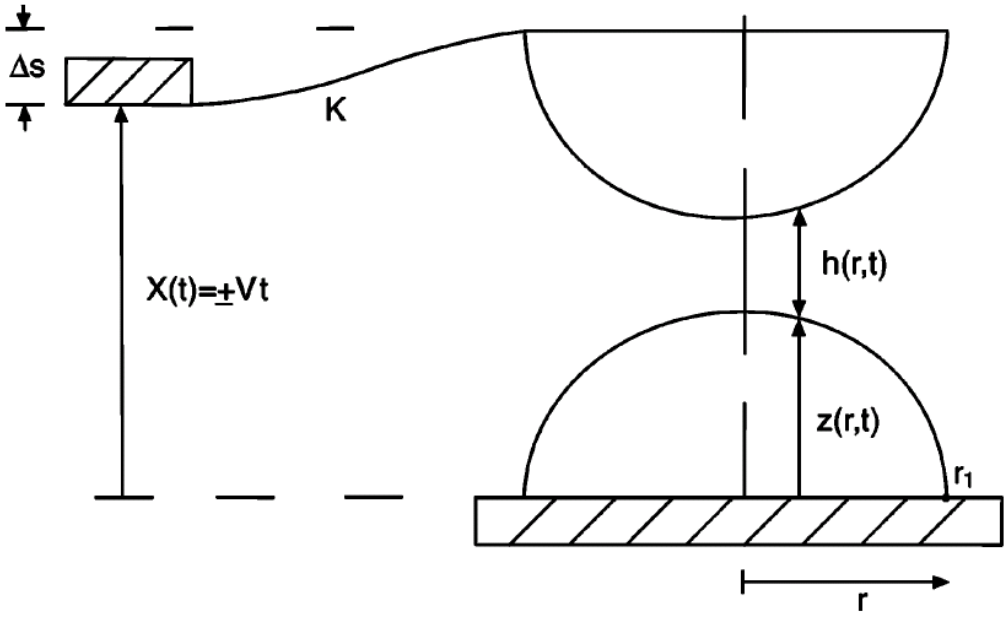

Klaseboer et al. (*J. Coll. Interface Sci.*, **229**, 274–285, 2000) have considered the case of *mobile* interfaces in the same geometry, but at rather longer length scales (10^{-3}m) where a planar approximation for the tangential stress is appropriate. The IFR implementation of this analysis has been stymied by numerical difficulties. Nevertheless, it remains unclear if such an approach is valid for the microscopic droplet sizes of interest (10^{-6}m). Moreover, it is known (IFR work) that protein stabilised interfaces especially can exhibit a significant dynamic response arising from interfacial viscosities, elasticities and tension gradients that contribute to discontinuities in both the tangential and normal stress components at the boundary.

We seek an extended theory that combines the virtues of the Carnie et al. model in describing the AFM experiment and the numerical robustness of their novel radial boundary condition, with a more general formulation that accounts for interfacial momentum transfer.

2.1.2 Dissipative interface rheology studied by pendant drop shape analysis (R. Penfold and P. Wilde)

In the absence of surface adsorbed contaminants, the mechanical properties of an equilibrium interface between two immiscible fluids is simply determined by a single coefficient: the interfacial tension γ that is isotropic, spatially uniform and time independent. The experimental determination of γ by axisymmetric drop shape analysis (ADSA) has a long history (Hoofar and Neumann, *Adv. Coll. Interface Sci.* **121**, 25–49 2006) and relies entirely on assuming that the profile of a fluid-fluid interface in a gravitational field arises from a force balance between weight, boundary tension and an excess pressure ΔP due to the local curvature (principal radii R_1 and R_2) given by the Laplace equation,

$$\Delta P = \gamma \left(\frac{1}{R_1} + \frac{1}{R_2} \right) \quad .$$

Although the mathematical formulation of the mechanical problem is straightforward, a very substantial literature exists concerned mainly with the development of robust numerical solution procedures, sensitivity analysis, error handling and experimental image processing of interface profiles.

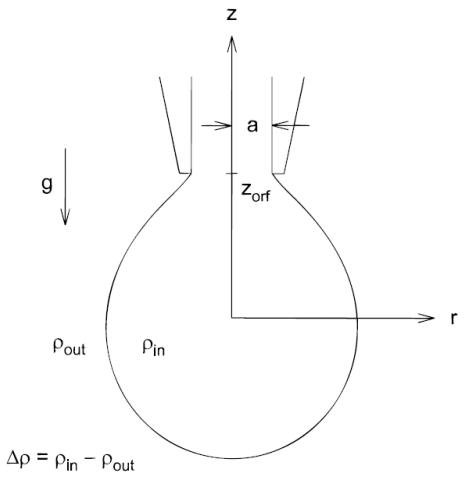

In practice, however, the interfacial tension of a clean fluid junction at mechanical equilibrium holds little scientific or technological interest. The ADSA method is much more widely used, and at IFR in particular, to interrogate the properties of interfaces where all manner of surface active agents have been absorbed – most notably multicomponent mixtures of carbohydrates, proteins, enzymes or metabolites. In general, such interfaces exhibit complicated dynamic surface rheology where both viscous and elastic contributions are important in the relevant frequency range. This rich dynamic behaviour can be a consequence of compositional variations driven by exchange fluxes between interface and bulk, or by intrinsic dissipative relaxation processes taking place within the surface. Oscillating pendant drop or bubble experiments probe these dilatational phenomena, but a complete mathematical analysis of this situation is lacking. Attempts have appeared (Wantke and Fruhner, *J. Coll. Interface Sci.*, **237**, 185–199, 2001; Yeung et al., *Langmuir*, **13**, 6597–6606, 1997) to account for interfacial viscoelasticity by treating the surface as a two-dimensional Boussinesq fluid that is a projection of a distinct thermodynamic phase.

Recent ADSA studies at IFR involving emulsifiers of complicated saliva extracts have highlighted the urgent need to model the relationship between nontrivial interfacial rheology and the response of drop profiles to oscillatory volume perturbations.

2.2 Class (B)

2.2.1 Proteolysis patterns – predicting digestion products (Y. Alexeev and A. Watson)

The goal of the talk is to give general introduction to digestion processes in the stomach and possible ways of mathematical analysis of the protein digestion data. The talk is divided in four parts:

1) introduction to digestion processes;

2) data for analysis;

3) proposed ways of data analysis;

4) future plans.

A possible statistical approach for elucidating the specificity of the pepsin enzyme will be discussed. It is anticipated that this discrete problem might also succumb to combinatorial or graph theoretical methods that would appeal to the skills and interests of pure mathematicians.

2.2.2 Modelling intestinal luminal events - how good was your dinner and does it really matter? (R. Faulks)

Living organisms persist in a low entropy state that might be imagined as a saddle point on a multidimensional surface where the coordinate axes describe all manner of physical, biochemical and metabolic processes. In some "directions", nonlinear feedback controls allow the organism to recover homeostasis after small perturbations (e.g., in glyceamic index or lipid loading), while other excursions run away to catastrophic failure, pathology, disease or death. The situation is complicated by a temporal dimension with multiple over-lapping scales and cumulative threshold effects. We seek a process control theory that is applicable to biological systems.

A suitable starting point might be to consider a simple intestinal energy inventory. Although the calorific input can be easily defined, it is less clear what are the appropriate storage, conversion and dissipation mechanisms. The coupling between these processes also needs to be considered and the time dependent feedback controls that modulate them. Necessary and sufficient conditions for possible bifurcations to chaotic behaviour should be identified. The main goal at this stage is to establish a coherent problem specification that could be subject to mathematical formulation.

2.2.3 Solubilisation in Bile Salt Micelles (G. Rich)

Fats and oils form a significant part of our diet. Their hydrophobic nature means that they and many of their digestion products are insoluble in water. Absorption of lipids in the small intestine depends on their solubilization in the aqueous phase of the small intestine. This is achieved by bile salts, which aggregate to form micelles, into which lipids can be incorporated to form mixed micelles. These mixed micelles disaggregate at the intestinal wall. The released lipids diffuse into the intestinal cells and can then be absorbed into the body.

Micellarization of surface active molecules such as bile salts can be studied in a number of ways including using low concentrations of probe molecules whose properties depend on their environment. For example the fine structure of the fluorescent emission spectrum of pyrene depends on the polarity (specifically the dipole moments of surrounding molecules). When the fluorescent intensity ratio of two pyrene emission peaks F_R is plotted against bile salt concentrations C, which cover the concentration range over which micelles are starting to form, one obtains a sigmoid curve. I have found can be fitted to an integrated form of the logistic equation,

$$F_R(C) = F_R(0) + \frac{KF_{\max}}{K + \exp\bigl(-\alpha C F_{\max}\bigr)} \quad ,$$

where K and α are constants, which depend on the nature of the bile salts, and $F_{\max}$ is the maximal intensity ratio.

Bile salts are unusual in that at low concentrations their micelles contain few molecules, typically between two and four. I would like to model the process of the onset of formation of bile salt micelles taking into account their mutual affinity and aggregation number of the micelles. We could extend the model to mixtures of bile salts and mixed micelles of bile salts with firstly lipids and secondly with other molecules that are used in digestion studies/ present in the small intestine.

2.2.4 Mixing of saliva in the mouth (R. Penfold and P. Wilde)

The functions of saliva are primarily to aid digestion and to control oral microflora, both symbiotic and pathological. By moistening food, saliva helps to create the food bolus for effective swallowing. Salivary amylases and lipases also initiate the breakdown of starches and fats in the mouth. Human saliva is % 98 water but also contains electrolytes, proteins, mucus (polysaccharides and glycoproteins) and antibacterial agents including secretory IgA, lactoferrin and peroxidase, as well as whole bacterial cells. In the mouth, saliva is produced by six glands arranged in three pairs. The parotid glands, despite being the largest produce only about % 25 of whole saliva and are located in subcutaneous tissues towards the back of the mouth. The much smaller submandibular glands lie beneath the lower jaws and are responsible for some % 70 of whole saliva in the oral cavity. A mainly mucous secretion accounting for only % 5 of whole saliva is produced by the sublingual glands found beneath the tongue. The composition of material produced by each pair of glands varies considerably. In particular, work at IFR is concerned with the surface activity of statherin that functions biologically to inhibit the nucleation and growth of calcium phosphate minerals and is especially abundant in parotidal secretions. It has proved extremely difficult to formulate model salivas, primarily because purified statherin reconstituted in aqueous solution has very different rheological response from whole native saliva.

This raises the question of the efficiency of mixing flows, during mastication in the mouth, of input streams from six spatially separated and compositionally distinct sources. We seek a fluid dynamical model that can predict the spation-temporal distribution of glandular components in whole saliva secreted during mastication.

3 Selected Problems

3.1 Dynamic interface rheology studied by atomic force microscopy (AFM) (R. Penfold)

3.1.1 Preliminary analysis

Following Carnie et al. [1], we consider an axisymmetric droplet in a cylindrical polar coordinate system $(r,\ \theta, z)$ with unit unit vectors $\mathbf{e}_r$, $\mathbf{e}_\theta$ and $\mathbf{e}_z$. All field quantities are supposed independent of the polar angle θ so that the velocity, excess pressure and thickness of the draining film fluid (viscosity μ) are defined in accordance with the accompanying diagram,

$$\mathbf{u}(r,\ t) = u(r,\ t)\mathbf{e}_r + w(r,\ t)\mathbf{e}_z \quad , \qquad p = p(r,\ t) \quad , \qquad h = h(r,\ t) \quad ,$$

Furthermore, $z = 0$ is a plane of reflection symmetry so that the deformable interfaces of both droplets are specified by the "free" surface,

$$\eta = \eta(r,\ z,\ t) = z - \tfrac{1}{2}h(r,\ t) = 0 \quad .$$

Under the assumption of a thin draining film, we appeal to usual scaling arguments [2] and obtain the governing equations of lubrication theory,

$$p_r = \mu u_{zz} \quad , \tag{1}$$

$$p_z = 0 \quad , \tag{2}$$

along with the continuity requirement for incompressible flow,

$$\nabla \cdot \mathbf{u} = u_r + \frac{u}{r} + w_z = \frac{1}{r}\left(ru\right)_r + w_z = 0 \quad , \tag{3}$$

and the kinematic condition on the material surface,

$$\frac{\mathrm{D}\eta}{\mathrm{D}t} = \left(\frac{\partial}{\partial t} + u\frac{\partial}{\partial r} + w\frac{\partial}{\partial z}\right)\eta = -\tfrac{1}{2}h_t - \tfrac{1}{2}Uh_r + w = 0 \quad . \tag{4}$$

From symmetry arguments, this system is subject to the boundary conditions,

$$u_z = w = 0 \quad \text{on} \quad z = 0 \quad , \tag{5}$$

$$u_r = w_r = h_r = p_r = 0 \quad \text{on} \quad r = 0 \quad , \tag{6}$$

and also the far-field constraint,

$$p \to 0 \quad \text{as} \quad r \to \infty \quad . \tag{7}$$

A complete theory, as attempted by Klaseboer et al. [3], would couple the thin film drainage with flows generated inside the drop by transfer of momentum across the interface. This will involve boundary conditions on the velocity and stress fields. For the sake of simplicity, however, we propose to avoid solving the difficult internal flow problem by prescribing a plausible radial velocity ansatz on the interface. In particular, we intuitively imagine the internal droplet velocity field near the interface to be reminiscent of a 2D stagnation point flow about the z-axis, so we set,

$$u = U(r,\ t) = \kappa r \quad , \quad w = W(z,\ t) = -2\kappa z \quad \text{on} \quad z = h/2 + \epsilon \quad , \tag{8}$$

where ϵ is an infinitesimal indicating the droplet side of the interface.

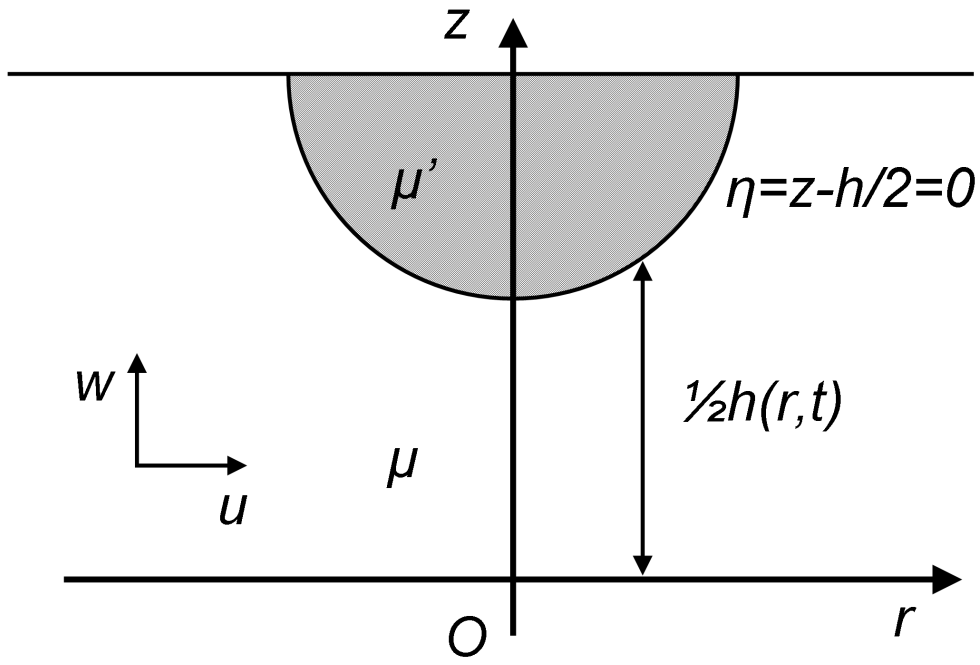

By virtue of the absent axial dependence of the pressure implied in (2), direct integration of (1) twice yields,

$$u = \frac{1}{\mu}\int\left(p_r\int \mathrm{d}z\right)\mathrm{d}z = \frac{p_r}{2\mu}\,z^2 + Az + B \quad .$$

The condition (5) immediately requires $A = 0$, while using (8) obtains the tangential velocity component in accord with eqn (3) of [3],

$$u = \frac{p_r}{2\mu}\left(z^2 - \left(\frac{h}{2}\right)^2\right) + U \quad , \tag{9}$$

so the flow divergence is,

$$\nabla\cdot\mathbf{u} = \frac{1}{2\mu}\left(\left(p_{rr} + \frac{p_r}{r}\right)\left(z^2 - \left(\frac{h}{2}\right)^2\right) - \frac{1}{2}p_r h h_r\right) + U_r + \frac{U}{r} + w_z \quad .$$

Integrating over the film thickness (i.e., a material balance) gives,

$$\begin{aligned}\int_{-h/2}^{h/2}\nabla\cdot\mathbf{u}\,\mathrm{d}z &= 2\int_0^{h/2}\nabla\cdot\mathbf{u}\,\mathrm{d}z\\ &= \frac{1}{\mu}\left(\frac{1}{r}\big(rp_r\big)_r\left(\frac{1}{3}-1\right)\left(\frac{h}{2}\right)^3 - \frac{1}{4}p_r h^2 h_r\right) + \frac{h}{r}\big(rU\big)_r + 2w|_{z=h/2}\\ &= -\frac{1}{12\mu r}\Big(\big(rp_r\big)_r h^3 + rp_r\big(h^3\big)_r\Big) + \frac{1}{r}\Big(\big(rU\big)_r h + rUh_r\Big) + h_t\\ &= 0 \quad ,\end{aligned}$$

where the boundary condition (5) has been observed and the kinematic condition (4) has been used to eliminate w. Solving for h_t finally gives the general Reynolds equation for this lubrication problem,

$$h_t = \frac{1}{12\mu r}\left(rh^3p_r\right)_r - \frac{1}{r}\left(rhU\right)_r = \frac{1}{r}\left(rh\left(\frac{h^2p_r}{12\mu} - U\right)\right)_r \quad , \tag{10}$$

in agreement with eqn (6) of Klaseboer et al. [3]. This should be supplemented by the initial condition,

$$h(r,\ 0) = h_0 + \frac{r^2}{R} \quad ,$$

where R is the undeformed drop radius and h_0 is the minimum interface separation at $t = 0$, taken so large that perturbations from spherical shape are negligible. Instead of invoking the kinematic condition, the stagnation flow ansatz can be used to eliminate $w|_{z=h/2} = -\kappa h$ and arrive at the ODE,

$$Uh_r + 2\kappa h = \frac{1}{r}\left(rh\left(\frac{h^2 p_r}{12\mu} - U \right) \right)_r \quad . \tag{11}$$

3.1.2 Discussion

From (9), the tangential stress on the film side of the interface is,

$$T_f = -\tau_f = \mu u_z\big|_{z=h/2} = \tfrac{1}{2} h p_r \quad , \tag{12}$$

and corresponds with eqn (4) of [3] but with a sign change accounting for the frictional drag felt by the interface that *opposes* draining flow. Progress here is hampered since T_f involves two unknown quantities: the film thickness h and radial component of the pressure gradient p_r.

In cylindrical coordinates with polar symmetry, the radial Navier-Stokes equation is,

$$U_t + UU_r + WU_z = \frac{1}{\rho'}\left(-P_r + \mu' \left(\frac{1}{r}\Big(rU_r \Big)_r - \frac{U}{r^2} \right) \right) \quad , \tag{13}$$

which simplifies for the stagnation point flow (8) to give,

$$\big(\dot\kappa + \kappa^2 \big) r = -\frac{P_r}{\rho'} \quad ,$$

and direct integration obtains the internal droplet pressure (near the interface),

$$P = P(r,\ t) = P_0 - \tfrac{1}{2}\rho' \big(\dot\kappa + \kappa^2 \big) r^2 \quad .$$

Combining this result with the excess pressure associated with the curvature of an immiscible fluid interface under tension σ leads to,

$$p = P - \frac{\sigma}{2r}\Big(rh_r \Big)_r \quad , \tag{14}$$

and hence the modified form,

$$h_t = -\frac{1}{r}\left(rh\left(\frac{h^2}{12\mu}\left(\rho'\big(\dot\kappa + \kappa^2 \big) r + \frac{\sigma}{2}\left(\frac{1}{r}\left(rh_r \right)_r \right)_r - \kappa r \right) \right) \right)_r \quad . \tag{15}$$

A more detailed analysis of a steady stagnation flow layer in a planar geometry suggests the ansatz,

$$U(r,\ z) = rf'(z) \quad , \quad W(z) = -f(z) \quad , \quad P(r) = \lambda \rho' r^2 \quad . \tag{16}$$

The idea that the bulk interior of the droplet remains quiescent is modelled by the boundary conditions,

$$U = W = 0 \ \text{ on } \ z = h + \epsilon \quad ,$$

while a prescribed stress τ_f is applied at the interface so that,

$$U_z = \frac{\tau_f}{\mu'} = \frac{Cr}{\mu'} \quad \text{on} \quad z = h \quad .$$

Again appealing to the Navier-Stokes equations (13), the steady ($U_t = 0$) tangential component of momentum balance gives a result of Falkner-Skan type [4],

$$r\left(\left(f'\right)^2 - ff''\right) = -2\lambda r + \frac{\mu'}{\rho'} rf''' \quad ,$$

whence we obtain the fourth order ODE,

$$\frac{\mu'}{\rho'} f'''' + ff''' - f'f'' = 0 \quad ,$$

subject to,

$$f(h) = f'(h) = f(h+\epsilon) = 0 \quad \text{and} \quad f'(h+\epsilon) = \frac{C}{\mu'} \quad .$$

3.1.3 Conclusion

This difficult problem consumed a lot of time in verifying the results of other workers. Nevertheless, the ansatz of modelling the droplet fluid layer near the interface by an axisymmetric stagnation point flow appears to be novel and potentially fruitful.

3.2 Solubilisation in Bile Salt Micelles (G. Rich)

Two distinct routes for attacking this problem were immediately apparent:

1) seek steady-state solutions in a dynamical treatment of the chemical kinetics;

2) seek stationary states in a thermodynamic treatment of the free energy.

It was agreed that route (1) offered the most likely avenue of success, so that route (2) was abandoned at this stage.

3.2.1 Model 1: Homogeneous micelle formation

We consider the formation of a micellar aggregate in a dynamical process described by the chemical equation,

$$n\big[S\big] \underset{r}{\overset{f}{\rightleftharpoons}} \big[S_n\big] \tag{17}$$

where $n \in \mathbb{N}$ free surfactant molecules S combine to form a micelle S_n with a forward rate constant f, while a micelle dissociates back to free molecules with a reverse rate constant r. The volume concentration of moiety X is denoted $[X]$.

For algebraic convenience, we set $x = [S]$ and $y = \big[S_n\big]$, so the rate of reaction R is,

$$R = -\dot{x} = n\dot{y} \quad ,$$

where the *consumption* rate (negative) of x is a factor n times faster than the *creation* rate (positive) of y. In other words, to produce each moiety of type y requires n moieties of type x and we immediately obtain the conservation law,

$$\dot{x} + n\dot{y} = 0 \qquad \Rightarrow \qquad x + ny = C \quad , \tag{18}$$

for a given fixed total surfactant concentration C. To make progress, we shall invoke the important assumption that:

- the association mechanism is an *elementary* n-fold reaction (n-th order molecularity) where no intermediate states are involved.

In other words, we shall suppose that the experimental rate law is given directly by the stoichiometric equation (17). Within this assumption, the kinetic corollary of the law of mass action implies,

$$R = fx^n - rny \quad .$$

After using the conservation law (18) to eliminate y, we seek solutions of,

$$\dot{x} + fx^n + rx - rC = 0 \quad .$$

A convenient nondimensionalisation introduces the volume fraction of free surfactant $\phi = x/C \geq 0$ and measures time in units of the dissociation frequency $\tau = rt$. Hence, we get,

$$\frac{\mathrm{d}\phi}{\mathrm{d}\tau} + \chi^{n-1}\phi^n + \phi - 1 = 0 \quad , \tag{19}$$

where,

$$\chi = C\left(\frac{f}{r}\right)^{1/(n-1)} = CK^{1/(n-1)} > 0 \quad ,$$

is a suitably scaled total concentration involving the usual chemical equilibrium constant $K = f/r$. By differentiating (19) with respect to ϕ we have,

$$\frac{\mathrm{d}}{\mathrm{d}\phi}\left(\frac{\mathrm{d}\phi}{\mathrm{d}\tau}\right) = -\left(1 + n(\chi\phi)^{n-1}\right) \quad ,$$

and we conclude that $\mathrm{d}\phi/\mathrm{d}\tau$ is monotonically decreasing for all $\phi \geq 0$ in accord with the phase portrait sketched below. The stable equilibrium point ϕ_s behaves like,

$$\chi^{n-1}\phi_s^n + \phi_s - 1 = 0 \quad \Rightarrow \quad \phi_s \sim \begin{cases} 1 \quad , \quad \chi \ll 1 & \Rightarrow \quad x \to C \\ \chi^{(1-n)/n} \quad , \quad \chi \gg 1 & \Rightarrow \quad x \to (C/K)^{1/n} \end{cases} \quad \text{as} \quad t \to \infty \quad .$$

The limiting cases can be formally verified by appealing to infinite series solutions of algebraic equations. In particular, for the trinomial above, the analysis of Lewis [5] shows that,

$$\phi_s = 1 - \chi^{n-1} + \sum_{s=2}^{\infty} \binom{ns}{s} (-\chi)^{s(n-1)} \quad , \quad \chi < \frac{1 - 1/n}{n^{1/(n-1)}} < 1 \quad ,$$

$$\phi_s = \chi^{(1-n)/n} - \frac{1}{n}\chi^{2(1-n)/n} + \frac{1}{n}\sum_{s=2}^{\infty} \frac{(-1)^s}{s!} \prod_{k=1}^{s-1} \left(\frac{1+s}{n} - k\right) \chi^{(1+s)(1-n)/n} \quad , \quad \frac{1 - 1/n}{n^{1/(n-1)}} < \chi \quad .$$

This is consistent with our intuition that a small equilibrium constant ($\chi \ll 1$) suppresses the formation of micelles and most of the available surfactant exists as free molecules $x \to C$ in the

steady state ($t \to \infty$). On the other hand, if the forward reaction rate dominates so that the equilibrium constant is large ($\chi \gg 1$) then almost all the available surfactant is converted into micelles,

$$y = \frac{C-x}{n} \to \frac{1}{n}\left(C - \left(\frac{C}{K}\right)^{1/n}\right) \approx \frac{C}{n} \quad \text{as} \quad t \to \infty \quad ,$$

in the steady state.

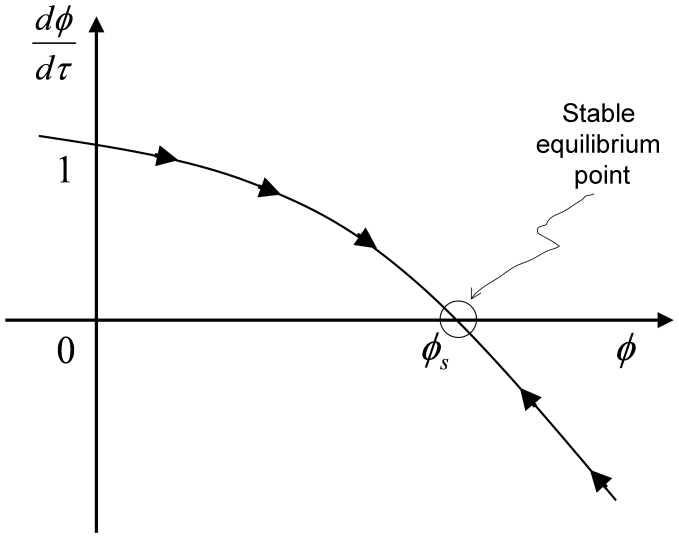

At dynamic equilibrium we have,

$$\left.\frac{\mathrm{d}\phi}{\mathrm{d}\tau}\right|_{\phi=\phi_s} = 0 \qquad \Rightarrow \qquad \chi^{n-1}\phi_s^n + \phi_s - 1 = 0 \quad , \tag{20}$$

and differentiating with respect to χ obtains,

$$\begin{aligned} &(n-1)\chi^{n-2}\phi_s^n + \left(n\big(\chi\phi_s\big)^{n-1} + 1\right)\frac{\mathrm{d}\phi_s}{\mathrm{d}\chi} = 0 \quad , \\ \Rightarrow \qquad &\frac{\mathrm{d}\phi_s}{\mathrm{d}\chi} = -\frac{(n-1)\phi_s\lambda^{n-1}\phi_s^n}{\lambda\left(\phi_s + n\lambda^{n-1}\phi_s^n\right)} = -\frac{\phi_s\big(1-\phi_s\big)}{\lambda\big(R_n - \phi_s\big)} \quad , \end{aligned} \tag{21}$$

where we have used the stationarity condition (20) and introduced $1 < R_n = n/(n-1) \leq 2$. It follows from (21) that $\mathrm{d}\phi_s/\mathrm{d}\chi < 0$ for all ϕ_s, so the equilibrium volume fraction of free surfactant is monotonically decreasing with concentration. Similarly, the equilibrium volume fraction of micelles is monotonically increasing with concentration. Moreover, in the limit of vanishingly small volume fraction we find,

$$\lim_{\phi_s \to 0} \frac{\mathrm{d}\phi_s}{\mathrm{d}\chi} = \begin{cases} -1 & , \quad n = 2 \\ 0 & , \quad n > 2 \end{cases} \quad .$$

Hence, for physically relevant aggregation numbers ($n > 2$), a sigmoidal form is predicted for the concentration dependence of the steady state free surfactant volume fraction (see figure). This appears to be consistent with the experimental observation.

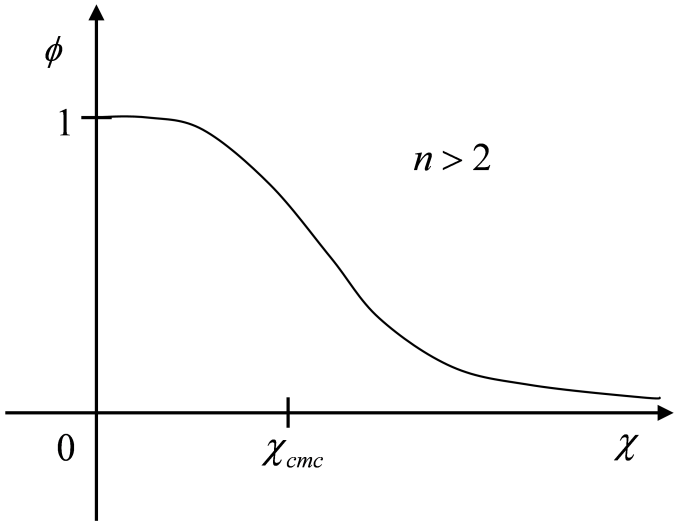

Differentiating (20) again yields,

$$\frac{\mathrm{d}^2\phi_s}{\mathrm{d}\chi^2} = -\frac{1}{\lambda^2\big(R_n-\phi_s\big)^2}\left(\big(1-2\phi_s\big)\,\frac{\mathrm{d}\phi_s}{\mathrm{d}\chi}\,\chi\big(R_n-\phi_s\big) - \left(R_n-\phi_s-\chi\,\frac{\mathrm{d}\phi_s}{\mathrm{d}\chi}\right)\phi_s\big(1-\phi_s\big)\right)$$
$$= \frac{2\phi_s\big(1-\phi_s\big)}{\lambda^2\big(R_n-\phi_s\big)^3}\left(\phi_s^2 - 2R_n\phi_s + \tfrac{1}{2}R_n\big(1+R_n\big)\right) \quad , \tag{22}$$

and we obtain the single non-zero inflection point,

$$\left.\frac{\mathrm{d}^2\phi_s}{\mathrm{d}\chi^2}\right|_{\phi=\phi_{cmc}} = 0 \qquad \Rightarrow \qquad \phi_{cmc} = R_n - \sqrt{\tfrac{1}{2}R_n\big(R_n-1\big)} = \frac{n-\sqrt{\frac{1}{2}n}}{n-1} \quad ,$$

where the equilibrium rate of micelle production is maximal. We therefore interpret the corresponding critical micelle concentration,

$$C_{cmc} = \left(\frac{1-\phi_{cmc}}{K\phi_{cmc}^n}\right)^{1/(n-1)} \quad , \tag{23}$$

and observe that this quantity depends only on the equilibrium constant K and the aggregation number n.

3.2.2 Model 2: Inhomogeneous micelle formation

A straightforward generalisation of Model 1 accounts for the formation of mixed micelles by the post-aggregation coalescence of different homogeneous micelles. Under the same principal assumption of elementary multi-molecular reactions, we propose the extended scheme,

$$n_1\big[S^{(1)}\big] \underset{r_1}{\overset{f_1}{\rightleftharpoons}} \big[S_{n_1}^{(1)}\big] \quad ,$$
$$n_2\big[S^{(2)}\big] \underset{r_2}{\overset{f_2}{\rightleftharpoons}} \big[S_{n_2}^{(2)}\big] \quad ,$$
$$\big[S_{n_1}^{(1)}\big] + \big[S_{n_2}^{(2)}\big] \underset{r}{\overset{f}{\rightleftharpoons}} \big[S_{n_1+n_2}\big] \quad ,$$

with the corresponding reaction rates rendered in a natural algebraic notation,

$$\begin{aligned} R_1 &= -\dot{x}_1 = n_1\big(\dot{y}_1 + \dot{y}\big) = f_1 x_1^{n_1} - n_1 r_1 y_1 \quad , \\ R_2 &= -\dot{x}_2 = n_2\big(\dot{y}_2 + \dot{y}\big) = f_2 x_2^{n_2} - n_2 r_2 y_2 \quad , \\ R &= -\left(\dot{y}_1 + \frac{\dot{x}_1}{n_1}\right) = -\left(\dot{y}_2 + \frac{\dot{x}_2}{n_2}\right) = \dot{y} = f y_1 y_2 - r y \quad . \end{aligned}$$

The corresponding material conservation laws are obtained immediately,

$$\begin{aligned} \dot{x}_1 + n_1\big(\dot{y}_1 + \dot{y}\big) = 0 \quad &\Rightarrow \quad x_1 + n_1\big(y_1 + y\big) = C_1 \quad , \\ \dot{x}_2 + n_2\big(\dot{y}_2 + \dot{y}\big) = 0 \quad &\Rightarrow \quad x_2 + n_2\big(y_2 + y\big) = C_2 \quad , \end{aligned}$$

and can be used to eliminate the intermediate homogeneous micelle variables y_1 and y_2 thus,

$$\begin{aligned} \dot{x}_1 + f_1 x_1^{n_1} + r_1\big(x_1 - n_1 y\big) - r_1 C_1 = 0 \quad , \\ \dot{x}_2 + f_2 x_2^{n_2} + r_2\big(x_2 - n_2 y\big) - r_2 C_2 = 0 \quad , \\ \dot{y} + r y - f\left(\frac{C_1 - x_1}{n_1} - y\right)\left(\frac{C_2 - x_2}{n_2} - y\right) = 0 \quad . \end{aligned}$$

In the steady state we obtain,

$$n_1 n_2 y = n_2\Big(C_1 - x_1 - K_1 x_1^{n_1}\Big) = n_1\Big(C_2 - x_2 - K_2 x_2^{n_2}\Big) = K_1 K_2 K x_1^{n_1} x_2^{n_2} \quad .$$

3.2.3 Conclusion

Model 1 predicts a micelle aggregation profile that is qualitatively in agreement with observations. The experimental results are rather more complicated in that the micelle formation process is only inferred indirectly by the fluorescence change of a marker molecule (pyrene) in passing from a hydrophilic to a hydrophobic environment. Unsurprisingly, however, the aromatic conjugation of pyrene that is exploited here also leads to very low solubility in aqueous phases. For this reason, the saturation of the fluorescence ratio signal at high concentration may not be directly interpreted as complete micellisation. Nevertheless, it should be possible to assess the validity of Model 1 by *lowering* the pyrene concentration and focusing on the dilute surfactant limit below the CMC.

The principal weakness of both models lies in the assumption of arbitrary molecularity for the physical aggregation mechanism. In reality, it is extremely unlikely that elementary reaction processes proceed by anything other than unimolecular or bimolecular steps, even in condensed phases. A more plausible scheme would involve all the *sequential* equilibria,

$$\begin{aligned} 2\big[S\big] &\underset{r_1}{\overset{f_1}{\rightleftharpoons}} \big[S_2\big] \quad , \\ \big[S\big] + \big[S_2\big] &\underset{r_2}{\overset{f_2}{\rightleftharpoons}} \big[S_3\big] \quad , \\ \big[S\big] + \big[S_3\big] &\underset{r_3}{\overset{f_3}{\rightleftharpoons}} \big[S_4\big] \quad , \\ \vdots \quad &\quad \vdots \quad \quad \vdots \\ \big[S\big] + \big[S_{n-1}\big] &\underset{r_{n-1}}{\overset{f_{n-1}}{\rightleftharpoons}} \big[S_n\big] \quad , \end{aligned}$$

though this brings the modelling disadvantage of proliferating the number of rate constant parameters.

3.3 Modelling intestinal luminal events - how good was your dinner and does it really matter? (R. Faulks)

A simple high-level description of the body weight regulation and composition is represented in the following diagram. Here the boxes denote the power associated with the chemical potential energy of digested nutrients as well as the chemical and physical work done to support healthy life. The ovals denote the temporally variable components of body mass, and the arrows suggest fluxes associated with metabolic processes. The prescribed energy input rate is characterised by the calorific content and time dependent composition (fat,carbohydrate and protein) of the diet, while the output rate might be regarded as the accumulation of oxidation processes involved in metabolic activity. Glycogen (sugar) is the animal cell analogue of starch in plants and can be regarded as the principal immediately available fuel source for the organism. Metabolic pathways exist for the cellular synthesis of glycogen from both protein and lipids as shown in the diagram. Similarly, the longer term storage of energy ("charging") in the more compact form of triglycerides (lipids) is controlled by the metabolic fluxes of de novo lipogenesis and the production of glyceraldehyde 3-phosphate that is a major intermediate for fixing carbon in plants and depositing adipose tissue (fat) in animals.

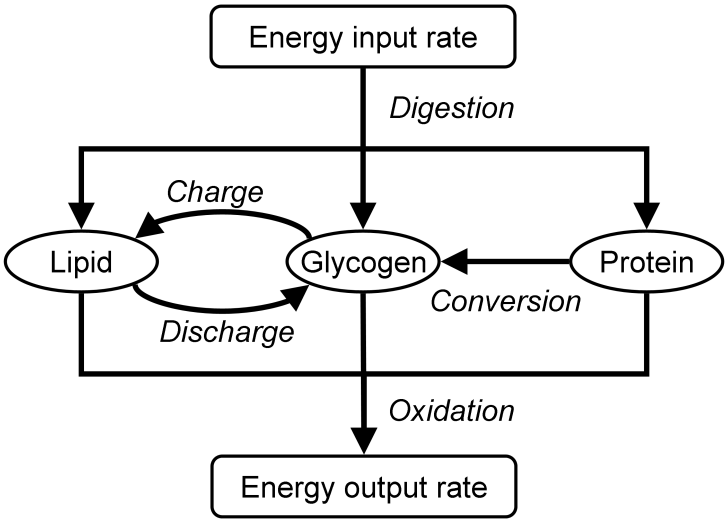

The mathematical realisation of this picture gives rise to a dynamical system that describes the time evolution (trajectory) of a point (vector of state variables) on a manifold (phase space), which is governed by deterministic rules. Here, this will amount to a system of coupled ordinary differential equations with constraints adopting the general form,

$$F(x,\ \dot{x}) = 0 \quad .$$

To construct such a model requires considerable non-mathematical insight into the biological nature of the problem. For example, Hall [6] has made some progress in this direction to arrive at a system of the form,

$$\begin{aligned}
\dot{L} &= L_i + \phi_c(L, \dot{L},\ G) - \phi_d(L, \dot{L},\ G) - L_o(L,\ \dot{L},\ G,\ \dot{G},\ P,\ \dot{P},\ T) \quad , \\
\dot{G} &= G_i - \phi_c(L, \dot{L},\ G) + \phi_d(L, \dot{L},\ G) - G_o(L,\ \dot{L},\ G,\ \dot{G},\ P,\ \dot{P},\ T) \quad , \\
\dot{P} &= P_i - \phi_x(P) - P_o(L,\ \dot{L},\ G,\ \dot{G},\ P,\ \dot{P},\ T) \quad , \\
\dot{T} &= \phi_t(T) \quad ,
\end{aligned}$$

where $L = L(t)$, $G = G(t)$ and $P = P(t)$ are the body masses of lipid, glycogen and protein, respectively, with the prescribed input fluxes L_i, G_i and P_i. The rates of lipid charging and discharging are denoted ϕ_c and ϕ_d while ϕ_x is the protein conversion rate and the corresponding oxidation rates are indicated by L_o, G_o and P_o. Among other specific effects, Hall has also considered an adaptive thermogenetic feedback mechanism (controlled by the dimensionless variable T) whereby an energy imbalance (more output than input, that is starvation) is observed to modulate metabolic rates and oppose changes in overall body mass.

The skills of mathematicians can arguably contribute more usefully in the *analysis* of such dynamical systems, by considering both the structural and Lyapanov stability or by classifying the trajectories and orbits. In particular, the characteristic behaviour of trajectories as a function of the system parameters and the appearance of bifurcation points would be of fundamental importance in using the model to predict perturbation response and catastrophic failure in the context of organism health.

References

[1] Carnie, S. L., Chan, D. Y. C., Lewis, C., Manica, R. and Dagastine, R. R. (2005), *Langmuir*, **21**, 2912–2922.

[2] Ockendon, H. and Ockendon, J. R. (1995), *Viscous Flow*, Cambridge University Press, Cambridge.

[3] Klaseboer, E., Chevaillier, J. Ph., Gourdon, C. and Masbernat, O. (2000), *J. Coll. Interface Sci.*, **229**, 274–285.

[4] `http://en.wikipedia.org/wiki/Blasius_boundary_layer`

[5] Lewis, A. J. (1935), *Natl. Math. Mag.*, **10**, 80–95.

[6] Hall, K. D. (2006), *Am. J. Physiol. Endocrinol. Metab.*, **291**, E23–E37.